Pressure Drop Estimation for Polyamide 6 Flow through Spinnerets and Filters

A. Guštin,[1] A. Zupančič,[1] E. Mitsoulis[2]

[1]*Department of Chemical Engineering, Faculty of Chemistry and Chemical Technology, University of Ljubljana, Aškerčeva 5, 1001, Ljubljana, Slovenia*
[2]*School of Mining Engineering and Metallurgy, National Technical University of Athens, Zografou, 157 80, Athens, Greece*

Received 9 September 2004; accepted 10 June 2005
DOI 10.1002/app.23308
Published online in Wiley InterScience (www.interscience.wiley.com).

ABSTRACT: The pressure drop resulting from polyamide 6 flow through industrial spinnerets and wire-mesh filters was examined as a possible parameter for improving spinning process constancy with experimental techniques and a numerical approach. The rheological characterization of the polymer melt was performed with a capillary rheometer and a controlled-stress rotational rheometer equipped with a high-temperature oven cell. Measurements in a nitrogen atmosphere were carried out at different temperatures and at various moisture contents to determine the effect of the postcondensation process on the rheological properties of the polymer melt. These experiments were used to collect all basic material information necessary to fit the data with the purely viscous Cross model and the viscoelastic Kaye, Bernstein, Kearsley, Zappas (K-BKZ) model. A spinning pilot plant (consisting of an extruder, a gear pump, a pressure sensor, and a spin beam with several spin packs installed) was used to measure pressure drop values through industrial spinnerets and through two types of filters: (1) Dutch twilled weave filters and (2) sintered filters. Pilot plant tests on filters showed that in the examined range of melt throughputs, the pressure drop increased linearly with an increase in the melt flow rate for all the filters considered. The results with respect to the spinneret geometry led to the conclusion that the numerical simulations gave satisfactory predictions even for experimental data coming from complex systems such as spinning plants, as long as extensional properties were accounted for by the model. On the contrary, pressure drop predictions obtained from the Cross model underestimated the pilot plant values by approximately 20% because of the inability of the model to consider the extensional component of the flow. J Appl Polym Sci 100: 1577–1587, 2006

Key words: extrusion; polyamides; polycondensation; viscoelastic properties

INTRODUCTION

Polyamide 6 (PA6) is a very common polymer used in different fields ranging from textile and carpet production to special technical applications (tires, heat-resistant plastics, etc.). Textile spinning in particular is a very demanding process. Yarns are getting thinner from day to day, and the use of dyeing stuff sensitive to polymer inhomogeneities is the main reason for constant research for polymer improvement.

The PA6 textile spinning process, presented in Figure 1, can be summarized as follows. Polymer chips are fed to screw extruders and melted at temperatures of approximately 250–260°C. In the storage vessels, the chips are strictly kept under a flow of nitrogen with a constant dew point to guarantee a constant moisture content and to avoid at the same time PA6 oxidation. The polymer melt is then conveyed to a heated manifold, which is composed of several pipes departing to the single spinning positions. One gear pump, placed just before the spin packs, extrudes the melt through the spin packs into open air, transforming one single melt stream into many thin filaments. Filaments are finally cooled in the open air and wound in bobbins.

One of the important parameters that can be related to the constancy of the yarn quality is the pressure drop measured through the spin pack because it directly depends on the filtration grade chosen for polymer purification. Figure 2(a,b) shows the three main elements composing a typical textile spin pack: a porous packed bed of steel particles, a filter, and a spinneret.

The aim of the porous packed bed and the filter is to stop extraneous particles present as impurities in the polymer melt and to break possible gels,[1] whereas the spinneret generates high shearing conditions on the

Correspondence to: A. Zupančič (andreja.valant@fkkt.uni-lj.si).

Contract grant sponsor: Slovenian Research Agency; Slovenian Ministry of Economy; contract grant number: 3311-03-831805.

Contract grant sponsor: General Secretariat of Science and Technology of Greece; contract grant number: 047-g.

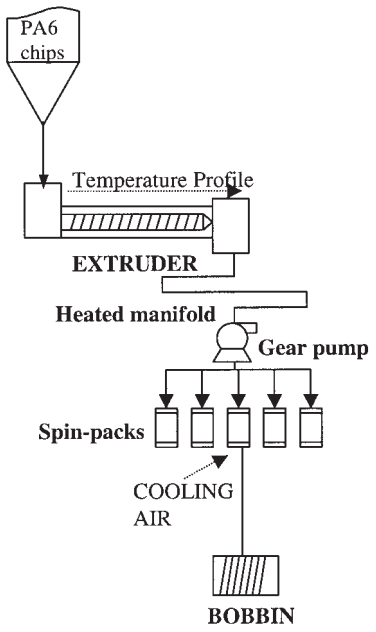

Figure 1 Schematic diagram of the textile spinning process.

polymer and splits the main flow into many very thin filaments. Depending on the packed bed granulometry, in the range of 100–200 μm, and on the filter opening dimensions, in the range of 10–40 μm, different pressure drop profiles will be achieved along the spin pack. Too high or too low a filtration grade can be both problematic: in the first case, the filters will clog very fast and will consequently need to be replaced frequently in production, whereas in the second case, the retention capacity of the filtering element will be so low that some particles could pass and break the yarn during extrusion. Sudden pressure drop changes could also cause problems in the final product quality because, depending on the cause, defects in yarn dyeability can result.

This work focuses in particular on the problem of pressure drop estimation through spinnerets and wire-mesh filters, two geometries that exhibit notable differences with respect to fluid dynamic behavior. In fact, although there is evidence of linear relationships between the pressure drop through porous media and the mass flow rate (Darcy's law), such a dependence cannot be assumed in the case of spinnerets because of the very small length/diameter (L/D) values characterizing their capillaries [Fig. 2(b)]. The flow pattern in this case has to be studied numerically, with consideration given to all the rheological aspects valid for not fully developed flow profiles at high shear rates through short dies.

The first fundamental aspects of non-Newtonian flow behavior through short dies are explained in Bagley's work.[2] Bagley described how to evaluate the pressure drop for different polyethylene melts when end effects could not be neglected. Since then, many studies have been performed,[3–7] mainly with polyolefins because of their industrial importance. Numerical simulations have followed with various degrees of success.[8–11] It appears that no articles have been published so far on pressure drop estimation for polymers derived from polycondensation reactions (polyamides in particular). The reason is that despite the great usage and long presence on world markets for PA6, its very complex rheology, resulting from postcondensation equilibrium reactions, and its propensity to oxidize in the presence of even small amounts of oxygen make this polymer difficult to use in investigations unless specifically required. This work attempts to rectify this situation, describing how rheological measurements, numerical simulations, and tests on pilot plants can be carried out to correctly estimate pressure drops through two particular geometries: spinnerets and filters.

The problem of the flow of Newtonian fluids through filters has been thoroughly studied in the past by several authors. Experiments carried out by Darcy proved the existence of a linear relationship between pressure drop Δp through a filtering cake of height L and throughput Q, with the slope of the line being a function of viscosity η, flow area A, and permeability factor K:

$$\frac{\Delta p}{L} = \frac{\eta}{AK} Q \tag{1}$$

The growing importance of porous medium geometry in many industrial segments, which has been observed in the last years, in combination with the availability on the market of a wide variety of polymers with peculiar fluid flow properties, has convinced several authors to reexamine the flow through this geometry for some of the industrially most relevant non-Newtonian fluids.[12] In these works, mainly two opposite techniques have been used to describe the flow through a packed bed of particles:

1. The microscopic technique, consisting of the study of the flow path at the pore level.

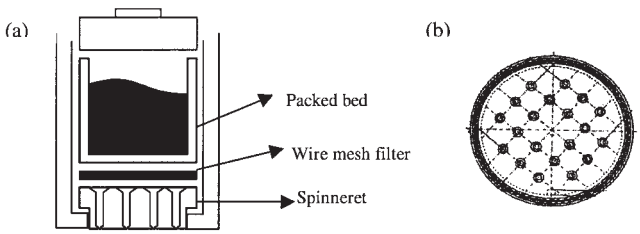

Figure 2 (a) Spin pack containing a spinneret, a filter, and a packed bed of steel particles and (b) frontal view of a spinneret.

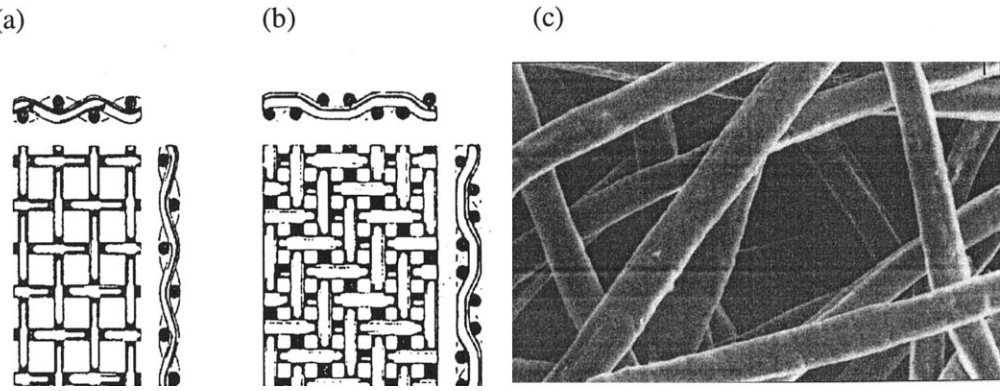

Figure 3 (a) PW filter, (b) DTW filter, and (c) magnified view of a sintered filter.

2. The macroscopic technique, in which the flow system is described in terms of overall measurable parameters such as the pressure drop and recovery efficiency.

In the microscopic methods, the flow through porous beds of particles is usually visualized with photomicrography techniques, and local properties in the pores are studied with the aim of getting all the necessary information for the definition of a predictive model for the macroscopic behavior of the system.

All of these considerations may be extended to the filter geometry, which is a particular type of porous medium. In textile production, mainly two types of filters are used: mesh filters and sintered filters.

Dutch twilled weave (DTW) filters are a particular class of mesh filters used in industrial spinning, and they are characterized by having openings all of the same dimensions and differing from the standard plane weave (PW) filters with typical square openings, in that two lines of wires are interweaved alternately instead of each single line being interweaved alternately [Fig. 3(a,b)]. This particular manufacturing procedure gives DTW filters a higher density of the weave, which results in a higher mechanical strength and in a different orientation of the openings, which allow the fluid to pass through the filter horizontally but not in the direction orthogonal to the plane of the filter.

The second class of filters [sintered filters; Fig. 3(c)] are produced from small steel fibers air-webbed to form a random mat and successively sintered to achieve a resistant matrix.[13] A result of the random disposition of the fibers in the mat is that the sintered filter opening dimensions are not uniform, but they are usually described by a distribution curve. Despite the great structure differences between DTW and sintered filters, when it comes to industrial applications, both of them meet the production requirements of a long onstream lifetime and short resistance to polymer flow because of their high porosity (60–85% for DTW filters and 48–52% for sintered filters) and high dirt-holding capacity.[13]

In the next sections, the pressure drop through filters and spinnerets is studied for the particular case of PA6 flow. Polyamides are polymers derived from polycondensation reactions, and this makes them very sensitive to the moisture content, temperature, and time (history). According to the polycondensation equilibrium, should any changes in the concentrations of the products or reactants occur, the system will react, favoring either the forward reaction (polyamidation) or the inverse reaction (hydrolysis), which will in turn result in an increase or decrease of the polymer molecular weight. The temperature influences the polycondensation in two counteracting ways. As the temperature increases, the exothermic nature of the reaction will tend to favor the inverse reaction,[14] whereas at higher temperatures, faster polyamidation kinetics will be observed.[15]

These considerations were taken into account in the rheological characterization of PA6. From the experimental set of data, the material functions were determined, and the Cross and K-BKZ models were fitted. Numerical simulations of the flow of PA6 through spinnerets were performed on the basis of known geometries, material functions, and operating conditions. The measurements of the pressure drop on a pilot plant (with an introductory survey of the pilot plant layout and measurement setup) were compared with numerically predicted pressure drop values to check the reliability of the procedure. From pilot plant measurements, a trend common to all the examined filters, a pressure drop through the filter flow rate, was also identified and is discussed.

EXPERIMENTAL

Rheological measurements

Material determination

The polymer melt was an industrial-grade PA6 with the following properties: relative viscosity[16] = 2.44, NH_2 end group content[17] = 47 mequiv/kg, and COOH end group content[17,18] = 70 mequiv/kg.

Sample preparation

To obtain PA6 samples with different moisture contents, a representative sample of PA6 chips was milled and left to humidify for some hours at the ambient conditions. Afterwards, the powder was dried in a vacuum oven at 65°C for different residence times. Low temperatures and vacuum are essential when PA6 samples are dried to avoid their thermooxidative degradation (visible under a UV lamp[19]) or an increase in the molecular weight due to solid-phase polymerization.[20] Before the rheological measurements were started, the powder residual moisture contents were verified,[21] and the following moisture contents in PA6 were achieved: dry, 0.060%, 0.100%, and 0.140% (w/w).

Measuring equipment

The rheological characterization of the PA6 samples was carried out with a Physica MCR 300 controlled-stress rheometer (Graz, Austria) in the parallel-plate geometry (PP 30, gap = 1 mm). The rheometer was equipped with a high-temperature chamber and with a source of nitrogen, which guaranteed an inert atmosphere throughout the tests.

Measuring conditions and protocols

Rheological tests were carried out under nondestructive conditions of oscillatory shear in the range of the linear viscoelastic response. Measurements were performed at three temperatures: 230, 240, and 260°C. Although the lowest temperature was very close to the PA6 melting temperature (ca. 220–225°C)[18] and thus not interesting from a spinning point of view, nevertheless, it was found to be instructive to compare the polymer behavior at lower and higher polycondensation reaction rates (230 and 260°C, respectively). The rheometer was programmed to perform in a sequence in the same run isothermal time sweep tests [frequency (ω) = 10 Hz, strain (γ) = 0.10, time = 20 min] and frequency sweep tests (ω = 1–100 Hz, γ = 0.10) and to start recording data immediately after the sample loading. To achieve repeatable experimental data, a protocol of samples loading into the rheometer oven cell was preliminarily defined.

Rheological modeling

Two different constitutive models, the purely viscous Cross model[22] and the viscoelastic K-BKZ model proposed by Papanastasiou et al.[23] and modified by Luo and Tanner,[24] were fitted from the rheological data for numerical simulation purposes. It was convenient to use the Cross model in the numerical simulations at first because of its simplicity, its low computational cost (in comparison with complex viscoelastic models, e.g., the K-BKZ model), and its already proven suitability for simulating the flow of some polymers through short dies (e.g., for linear low-density polyethylene polymer melts[25]). Moreover, any differences with the viscoelastic K-BKZ results would reveal the relevance of the extensional properties in the flow through spinnerets.

TABLE I
Parameters of the Viscous Cross Model [Eq. (2)] for the PA6 Polymer at 260°C and with a 0.060% Moisture Content

Parameter	PA6
η_0	162.18 Pas
η_∞	0 Pas
K	0.0003244 s
n	0.0507

Cross model

The purely viscous Cross model in its complete form is described by the following four parameters: the asymptotic values of the viscosities at very low and very high shear rates, η_0 and η_∞, respectively, a constant parameter K with the dimensions of time, and a dimensionless constant n:

$$\frac{\eta - \eta_\infty}{\eta_0 - \eta_\infty} = \frac{1}{[1 + (K\dot{\gamma})^{1-n}]} \tag{2}$$

where $\dot{\gamma}$ is the shear rate. In our regression analysis, the term η_∞ has been neglected because there is no evidence of the existence of a second plateau in the high shear rate range, commonly found in the spinning process. All the other model parameters, given in Table I, were calculated from complex viscosity data collected during frequency sweep tests.

K-BKZ model

When typical viscoelastic phenomena, such as vortex creation at the capillary entrance or extrudate swelling at the capillary exit, become relevant, viscous models do not suffice any more for simulation purposes, and viscoelastic models have to be considered. As explained later, numerical simulations carried out with the commercial Fluent (Lebanon, NH) software package proved the unsuitability of the Cross model for simulating PA6 flow through spinnerets, forcing us to reconsider the problem by means of viscoelastic constitutive models. Among all the models available, the K-BKZ model was adopted for the calculations because of its wide use in the simulations of flow

TABLE II
Relaxation Spectrum for PA6 at 260°C and 0.060% with the K-BKZ Constitutive Equation [Eq. (3)]

k	λ_k (s)	a_k (Pa)
1	2.49×10^{-3}	1.54×10^{4}
2	1.34×10^{-4}	8.88×10^{5}
3	1.35×10^{-2}	2.31×10^{2}
4	3.51×10^{-1}	5.12×10^{0}
5	9.40×10^{3}	1.93×10^{-2}

$\alpha = 4.0792$; $\beta = 0.139$; $\theta = 0$.

through short dies.[8–11] In tensor notation, it gives the stress (τ) as follows:

$$\tau = \frac{1}{1-\theta}\int_{-\infty}^{t}\sum_{k=1}^{N}\alpha_k\lambda_k \exp\left(-\frac{t-t'}{\lambda_k}\right)\frac{\alpha}{(\alpha-3)+\beta I_{C^{-1}}+(1-\beta)I_C}\times[C_t^{-1}(t')+\theta C_t(t')]\,dt' \quad (3)$$

where λ_k and a_k are the relaxation time and relaxation modulus coefficients, respectively; N is the number of relaxation modes; and I_C and $I_C{}^{-1}$ are the first invariants of the Cauchy–Green tensor $\mathbf{C_t}$ and the Finger strain tensor $\mathbf{C_t}^{-1}$. Material properties in eq. (3) are accounted for by α and β (material constants) and by θ, which is defined as follows:

$$\frac{N_2}{N_1} = \frac{\theta}{1-\theta} \quad (4)$$

where N_1 and N_2 are the first and second normal stress differences, respectively.

The relaxation spectrum parameters λ_k and a_k, appearing in eq. (3), may be determined from a nonlinear regression of the experimental loss modulus (G'') and storage modulus (G') data.[26] The model parameters are shown in Table II.

Pilot plant measurements

Pilot plant layout

The pilot plant used in the tests had the same layout as the industrial spinning system shown in Figure 1, and so it consisted of the following main elements: a melting extruder, one gear pump assuring a constant melt flow rate, and a spin beam with installed spin packs. The experiments were monitored online by means of computer-controlled temperature and pressure sensors coupled to the system.

Pilot plant measurement setup

We carried out the experiments by mounting on the spin-beam spin packs of different compositions, recording the absolute pressure at the spin-pack inlet, and changing from time to time the melt flow rates. After six flow rates had been applied, the spin packs were replaced. At the very beginning of the experiments, the polymer residence time in the pilot plant was checked at a reference flow rate by the measurement of the time required for a tracer injected into the extruder inlet to flow out of the spinnerets. A constant system temperature (260 ± 1°C) and polymer moisture conditions (0.060 ± 0.010%) were ensured throughout the tests by online monitoring and by the storage of chips in silos under a flow of nitrogen of a constant temperature and dew point.

Two distinct series of tests were prepared. In the first series, spin packs containing only the spinnerets were prepared and installed, whereas in the second series of tests, the pressure drop through wire-mesh filters was studied. The mass flow rates referred per spinneret capillary were in the range of 0.8–3.3 g/min, enough to cover the spinneret shear rate range of 3500–15,000 s^{-1} and a polymer overall residence time range of 400–1100 s, both of them being wider than the interval of values found under normal industrial conditions. The results and observations reported in the next sections may thus be used as valid references in any industrial configuration.

In the experiments, two different types of spinnerets (L/D = 4.118 and 2.353) were chosen to give the highest and lowest pressure drop values at the melt throughputs studied. The throughputs per spinneret applied in both cases were the same in the range of 16–40 g/min. However, the first spinneret (L/D = 4.118; design 1) had 12 capillaries, whereas the second (L/D = 2.353; design 2) had 20 capillaries. After the spin-pack installation, the system required approximately 1 h to stabilize at the first flow rate because the polymer melt entering the spin packs had to first expel air from them and afterwards to cool them to the working temperature.

In the second part of the testing, DTW filters with filtration grades of 15, 25, and 43 μm and one sintered filter with an average filtration grade of 15 μm were analyzed, but because spin packs containing only filters could not be prepared, the overall pressure drop through the filters and spinnerets was measured. The pressure drop associated with the flow through filters was calculated a second time by the subtraction, from the overall pressure drop, of the spinneret contribution measured in the first series of tests.

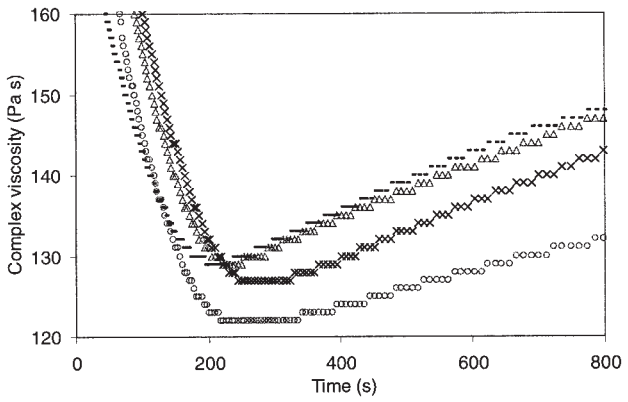

Figure 4 Time sweep tests (ω = 10 Hz, γ = 10%) showing the influence of the polycondensation reaction on the complex viscosity at 260°C for different moisture contents: (●) a dry sample, (△) 0.060%, (×) 0.100%, and (○) 0.140%.

RESULTS AND DISCUSSION

Rheological results

The progress in time of the postcondensation reactions occurring in the samples at a constant temperature was examined with time sweep tests under oscillatory shear conditions. Experimental data in Figure 4 indicate a common shape of the curves for all the samples, regardless of the temperature and moisture content. At the beginning of the time sweep tests (startup conditions), the complex viscosity decreased because of powder heating and melting; then, it reached a minimum and stayed constant for a short period until, in the third region, it started to increase with time. The increase in the complex viscosity had to be attributed to ongoing polycondensation reactions and in particular to the fact that all the samples had lower moisture contents than the equilibrium value. At 260°C, the displacement between the curves in Figure 4 resulted from different moisture contents: experimental data from the dry sample exhibited higher values, the uppermost curve, and the highest increase in the complex viscosity with time. The sample with the highest moisture content exhibited lower values of the complex viscosity, the lowermost curve, and the least pronounced increase in the complex viscosity with time. This type of behavior can be explained in terms of the polycondensation reaction process. In fact, the greater the gap was between the effective moisture content and polymer equilibrium moisture content, the steeper the viscosity increase was with time.

The curves of Figure 5 report frequency sweep results. They are arranged in the same way as discussed in the previous paragraph: at lower moisture contents, higher complex viscosity values were obtained in the whole frequency range under study. This is in agreement with trends measured by different experimental procedures and with PA6 data reported in the literature[27] and confirms the reliability of the applied experimental procedures and, therefore, the suitability of these data for numerical simulations.

Furthermore, for numerical simulations, it was necessary to obtain the viscosity function, that is, the shear viscosity versus the shear rate. According to Figure 6(a), the shear viscosity under destructive shear conditions and the complex viscosity curves superimposed with each other up to shear rates of 100 s^{-1} at any temperature and any moisture content (thus confirming the validity of the Cox–Merz rule also for polyamides[28]) when continuous and oscillatory data were compared at the same residence time. The shapes of both curves showed a quite broad Newtonian region in comparison with other polymer melts. At approximately 100 s^{-1}, the shear viscosity curves exhibited a steep viscosity drop, which could be attributed to polymer slippage and, more likely, to an inhomogeneous flow field. This was experimentally visible as a leakage of the polymer from the rheometer.

To reach higher shear rates encountered in spinning operations, we performed some measurements just on the sample with a humidity of 0.140% [Fig. 6(b)] with a Dynisco LCR 7000 capillary rheometer (the installed capillary had an L/D ratio of 40). The viscosity function superimposed with results from the rotational rheometer on the same Cross curve. There may be some doubt whether this was true for all the samples and moisture contents, although we can speculate that the superposition with the other samples could be expected.

The mechanical spectra of PA6 samples at various moisture contents and at different temperatures are illustrated in Figure 7. The frequency dependence of G'' showed the same trend for all samples at all temperatures, whereas through the variation of the moisture content, a deviation in the frequency dependence of G' in the low frequency range was observed at

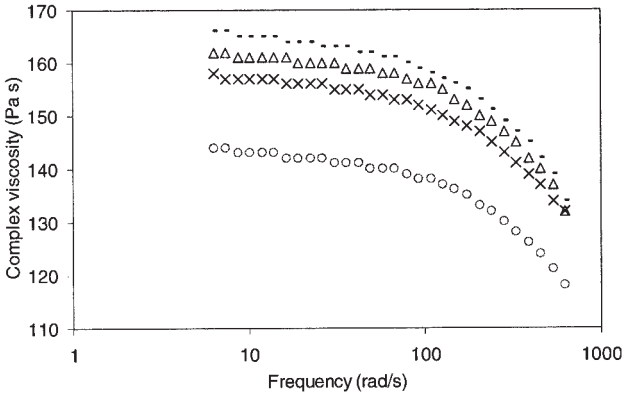

Figure 5 Frequency sweep tests showing the complex viscosity at 260°C for PA6 samples with different moisture contents: (- - -) a dry sample, (△) 0.060%, (×) 0.100%, and (○) 0.140%.

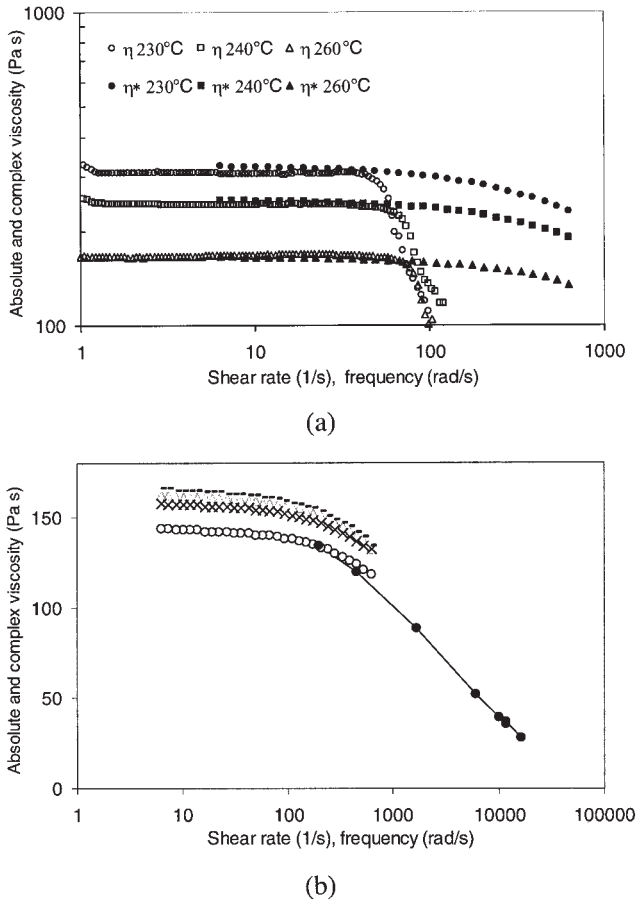

Figure 6 Shear viscosity (η) versus the shear rate and complex viscosity (η^*) versus the frequency for (a) a PA6 sample with 0.060 wt % moisture content at 230, 240, and 260°C and (b) PA6 data at 260°C showing superpositioning at a 0.140 wt % moisture content [rotational rheometer results: (- - -) a dry sample, (△) 0.060%, (×) 0.100%, and (○) 0.140%; capillary rheometer results: (●) 0.140%].

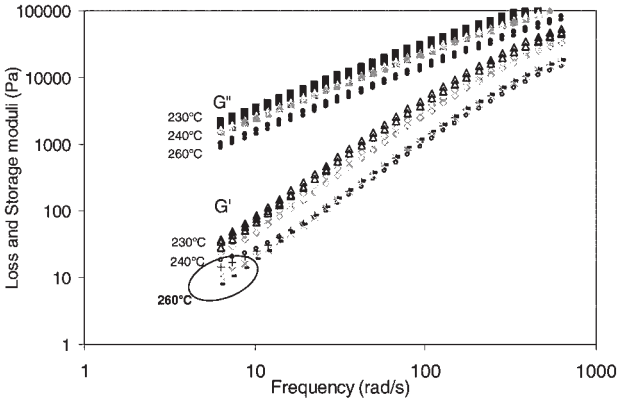

Figure 7 Frequency sweep test results (at 10% deformation) showing G' and G'' as functions of the temperature: (○) a dry sample, (+) 0.060%, (×) 0.100%, and (- - -) 0.140%. A deviation of G' at 260°C and at a higher residence time is shown as a function of the moisture content.

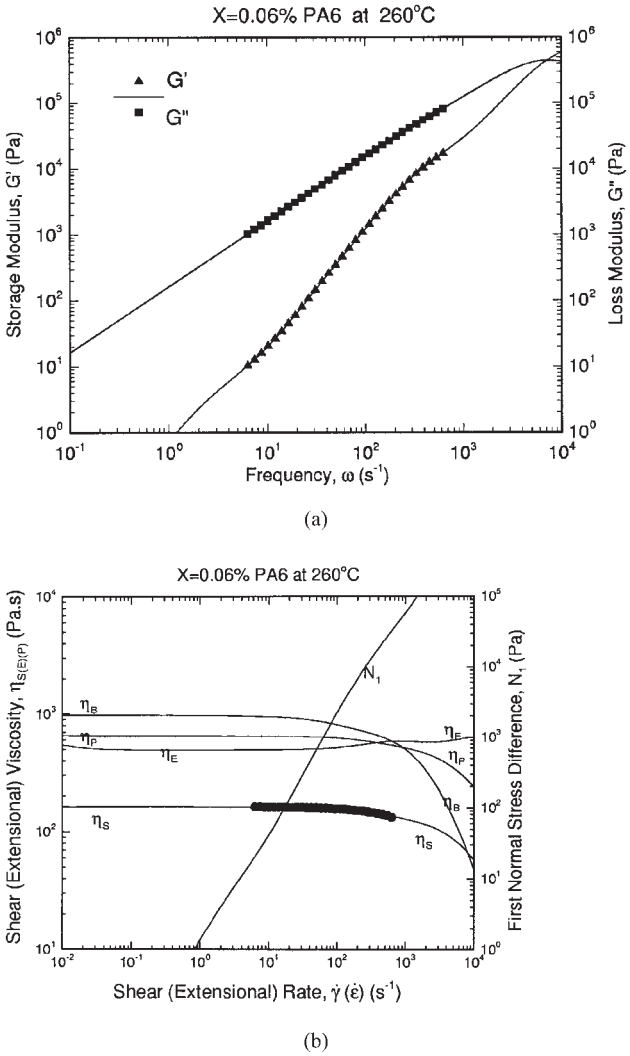

Figure 8 Calculated rheological properties for a sample with 0.060% moisture content after a residence time of 20 min at 260°C. The symbols show experimental data, whereas the lines show model predictions.

260°C. This might be ascribed to faster polycondensation kinetics at 260°C, for which the residence time during measurements at low frequencies was long enough to discriminate the behavior according to the moisture content.

Rheological modeling

With these reported results, the Cross and K-BKZ model parameters reported in Tables I and II were obtained. Figure 8 shows in a graphical form all the material functions obtained with the K-BKZ model to fit the data. These include the shear viscosity (η_S) and N_1 as functions of the shear rate $\dot{\gamma}$ and the uniaxial elongational viscosity (η_E), the planar extensional viscosity (η_P), and biaxial extensional viscosity (η_B) as functions of the extensional rate $\dot{\varepsilon}$. An interesting pa-

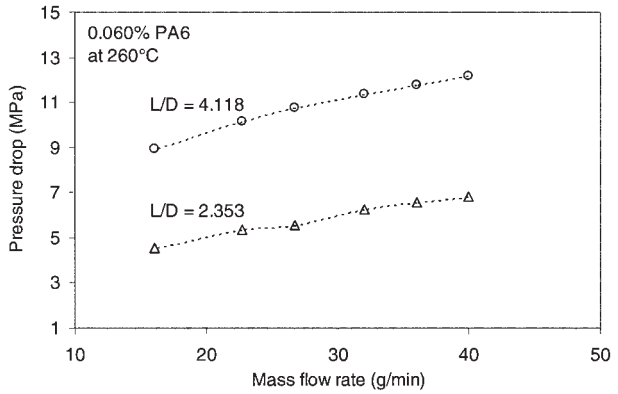

Figure 9 Pressure drop through spinnerets as a function of the flow rate for two die designs.

rameter that is usually obtained from the viscoelastic models is the Trouton ratio (T_R), which is defined as the ratio of η_E to η_S:[29]

$$T_R(\dot{\varepsilon}) = \frac{\eta_E(\dot{\varepsilon})}{\eta_S(\sqrt{3}\dot{\varepsilon})} \tag{5}$$

The values are calculated at different $\dot{\varepsilon}$ values. If the flow is inelastic (as with the Cross model), T_R is 3 for all values of $\dot{\varepsilon}$. For viscoelastic flows and for this PA6 with the data of Figure 8 and Table II, T_R is approximately 3 up to 100 s^{-1}, after which it rises substantially, thus signifying the onset of elongational effects on the flow.

Pilot plant results

Pressure drop through spinnerets

Figure 9 shows the results (pressure drops) obtained at six different mass flow rates for two spinnerets with L/D values of 4.118 and 2.353, which were specifically chosen to give the highest and lowest pressure drop values at the melt throughputs examined. The pressure drops were calculated as the difference between the spin-pack inlet pressure and spin-pack exit pressure, and a constant pressure value at the spin-pack exit (1 bar) was assumed because the polymer was extruded into the open air.

Pressure drop through filters

The experimental results of Figure 10 show that for the range of flow rates under study, a linear relationship can be assumed to calculate the associated pressure drop values. The linearity of this relationship is good because the precision of the pressure readings is ±1 bar and all regression lines pass (as they should) through the origin of the coordinate system. As expected, the curves in Figure 10 follow, with no exceptions, the principle that the smaller the filter openings are, the higher the pressure drop is for a fixed melt throughput. The highest results were in fact achieved for the 15-μm sintered filter because this is the only one among the filters examined that presents a fraction of openings smaller than 15 μm. This is in agreement with the linear trend observed in the study of the flow of xanthan gum through packed beds made of sand packs,[12] and we believe it is the result of two physical effects: the high porosity of the filters leading to low shear rates and the limited range of melt throughputs considered.

Numerical simulations

The problem of pressure drop estimation through spinnerets has been approached numerically with two CFD software packages [Fluent and homemade computational fluid dynamics (CFD) software called CAVES] and two different constitutive models for the description of the PA6 rheological properties: the Cross and K-BKZ models. Since spinnerets are made from capillaries having all the same dimensions, the problem has been reduced to the evaluation of the pressure drop through a single spinneret capillary (see Fig. 11). The capillary consists of four main regions (indicated in Fig. 11 with I, II, III, and IV); the last two (III and IV) are responsible for polymer stretching due to the tapered geometry. The geometry parameters of the two designs are given in Table III. The grids for the two designs are shown in Figure 12, in which a total of 700 elements have been used with the CAVES finite-element program. The lower part of each grid shows a denser grid with 4 times the number of elements on which trial runs were made to guarantee grid-independent results.

Numerical simulations were undertaken for both types of capillary designs, solving the conservation

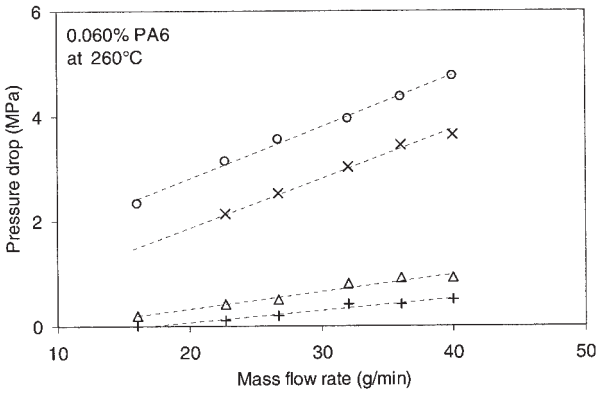

Figure 10 Pressure drop through different filters as a function of the flow rate: (○) 15-μm sintered filter, (×) 15-μm DTW filter, (△) 25-μm DTW filter, and (+) 40-μm DTW filter.

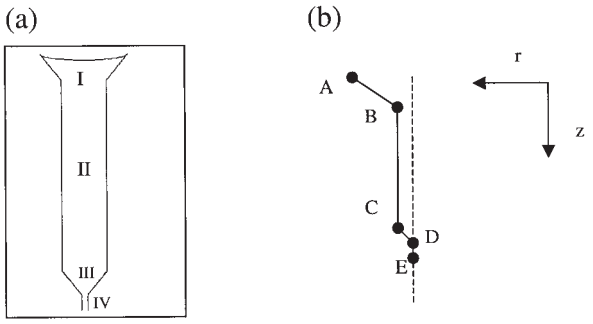

Figure 11 (a) Drawing of a spinneret capillary, showing four distinct regions (the regions responsible for polymer shearing and stretching are III and IV, respectively), and (b) coordinate system and design parameters (see also Table III).

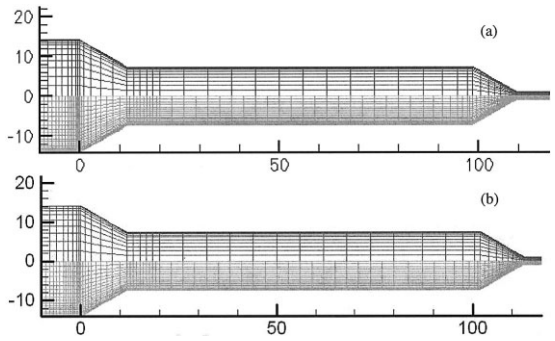

Figure 12 Finite-element grids used in the simulations: (a) design 1 and (b) design 2.

equations of mass and momentum together with either PA6 constitutive model. Incompressible fluid and isothermal flow conditions were also assumed, and the geometry of the capillary additionally was simplified by the consideration of only half of its section in the calculations due to axisymmetry. This allowed us to simulate with Fluent a three-dimensional flow with a mesh of 10^5 elements, which proved to be adequate for reaching convergence in a reasonable time.

Calculations were launched under the assumption of no slippage at the capillary walls and with the outlet absolute pressure and the inlet mass flow rate fixed as the operating variables.

Comparison of numerical simulation results with pilot plant experimental results

Viscous model

The first attempt to simulate the experimental pilot plant data was made with the Cross model as the rheological constitutive equation. To obtain satisfactory predictions, important experimental features, such as the viscosity dependence on the temperature, the shear conditions, and the residence time in the system, had to be accounted for properly. Knowing the relationship between the melt flow rate and overall residence time in the system, we fitted the Cross parameters separately at each flow rate, considering the associated residence time.

Reliable pressure drop predictions required, at each flow rate, approximately 6000–8000 iterations with Fluent, whereas only 100 iterations were necessary with CAVES. The differences in the iterations were due to the different numerical methods used (a finite-volume method with Fluent vs a finite-element method with CAVES). The flow patterns observed at a typical flow rate are shown in Figure 13 through the streamlines, isobars, and contours of the shear rate. A nice, smooth streamline pattern was obtained in this geometry with no vortex activity because of the tapered conical design. Most of the pressure drop occurred in the capillary die, whereas the reservoir had minimal pressure drop (same color in the reservoir). The shear rates were very high in the capillary wall

TABLE III
Geometric Parameters for the Two Designs of the Spinneret Capillaries Used in the Experiments and Simulations (See Also Fig. 11)

Drawing of a spinneret	Design	Coordinates (z, r)
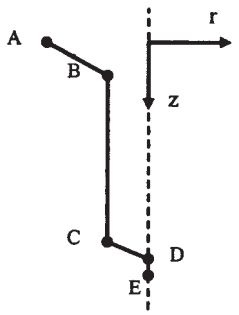	Design 1	A = (0, 2.405)
		B = (2, 1.25)
	12 capillaries	C = (16.73, 1.25)
	L = 1.4 mm	D = (18.6, 0.17)
	D = 0.34 mm	E = (20, 0.17)
	Design 2	A = (0, 2.405)
		B = (2, 1.25)
	20 capillaries	C = (17.33, 1.25)
	L = 0.8 mm	D = (19.2, 0.17)
	D = 0.34 mm	E = (20, 0.17)

The first number in parentheses refers to the z coordinate; the second refers to the r coordinate (mm). Initial conditions: pressure at the exit side (point E) = 1 bar.

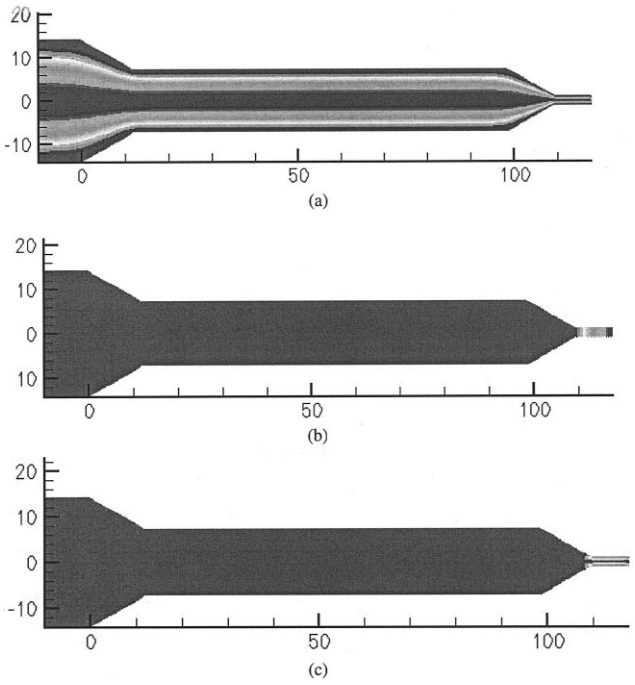

Figure 13 Typical flow patterns from the simulations in design 1: (a) streamlines, (b) isobars, and (c) shear rate contours.

and could reach up to 15,000 s^{-1}, whereas they remained quite low in the reservoir. These typical contour patterns helped us better visualize and understand the flow field inside the spinneret capillaries.

The tapered conical geometry of the die is the main reason that complex flow patterns (e.g., the creation of vortices) were not expected in these simulations. On the other hand, the lack of normal stresses in shear and the incorrect elongational viscosity inherent in the Cross model ($T_R = 3$ for all rates) are the main reasons that the underestimation of experimental pressure drop values was to be expected.

Our simulation results reported in Figure 14 for the two designs confirm this when we compare the Cross model predictions with the experimental data. The disagreement between the numerical predictions and experimental values is evident for both designs and increases more with the flow rate. The observed deviation is around 20%. An analysis of the distribution of the pressure drop along the capillary [see Fig. 13(b)] shows that almost the entire pressure drop is concentrated in the last region (IV). This is of course directly related to the differences in the geometrical parameters, particularly the much lower diameter of the IV region (ca. 8 times) in comparison with the diameter of the II region.

Viscoelastic model

Having proved the inability of purely viscous models to simulate correctly the flow of polyamides through spinnerets, we found it worthwhile to repeat the simulations with a viscoelastic model.

Pressure drop predictions obtained with the K-BKZ viscoelastic model are also reported in Figure 14. Axial velocity profiles similar to the ones obtained with the Cross model were found, showing no vortices at any flow rate. Nevertheless, because of the consideration of the extensional contributions inherent in the viscoelastic model, when T_R was greater than 3 and kept growing with the strain rate, a better agreement with the experimental results was achieved for both designs. In particular, at the lowest flow rate, both the viscoelastic predictions and experimental data agreed very well. After that, the viscoelastic simulations showed some discrepancies from the experiments, which increased with the flow rate in the order of 3% for design 1 and 9% for design 2 (short die). Still, these differences are quite acceptable, and so the adequacy of the viscoelastic K-BKZ model to correctly predict pressure drops in the spinneret for such polymer melts as PA6 is manifested.

CONCLUSIONS

The pressure drop resulting from PA6 flow through industrial spinnerets and wire-mesh filters was studied as a possible tool for improving the constancy of the spinning process. First, rheological measurements were carried out on a rotational rheometer to define all PA6 viscous and viscoelastic parameters, which were necessary for the fitting of the Cross and K-BKZ models. In this step, the rheological properties were analyzed as a function of ongoing polycondensation reactions, and the validity of the Cox–Merz rule was experimentally confirmed.

Pressure drop values arising from PA6 flow through spinnerets were then estimated; we solved numerically the flow for each of the two constitutive

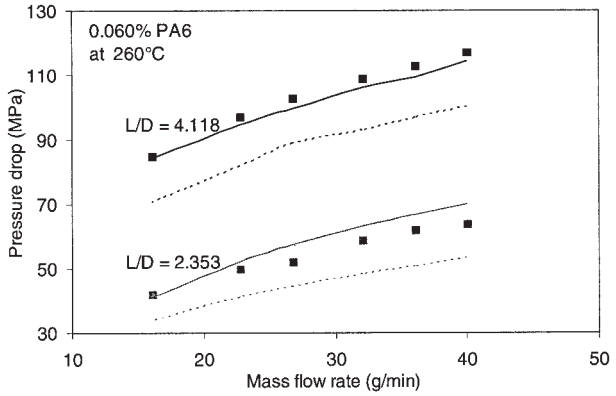

Figure 14 Comparison of (■) the experimental data and (—) the K-BKZ model and (- - -) Cross model simulations for the pressure drop through spinnerets as a function of the flow rate for two die designs.

models and compared the results to pressure drop values measured on an industrial pilot plant. A pilot plant consisting of a single screw extruder, a gear pump, a heated spin beam containing several spin packs, and a winder was used for this purpose. We carried out the experiments by installing into the spinning system spin packs containing either the mere spinnerets or a combination of spinnerets and filters and by recording the absolute pressure measured at the spin-pack inlet for different melt throughputs. A good agreement between the experimental results and K-BKZ model predictions was found, whereas underestimated results (up to 20%) were obtained with the Cross model at all flow rates examined because of its inability to simulate correctly the convergent flow pattern. In particular, it was found that an increasing T_R value (>3) at high strain rates, associated with high elongational viscosity, contributed substantially (ca. 20%) to the pressure drop increase.

Finally, pressure drops through DTW filters and sintered filters were also studied experimentally with the pilot plant described previously. Results from the pilot plant proved the existence of a linear relationship between the pressure drop values and melt flow rates for all the filters considered.

The authors are grateful to Julon Co. (a Slovenian company of the Gruppo Bonazzi Group) for the tests carried out on the pilot plant. They thank the Faculty of Pharmacy of the University of Ljubljana (Ljubljana, Slovenia), particularly S. Srčič and R. Dreu, for their support with the Fluent simulations. This work was carried out as a joint collaboration between Greece and Slovenia under the auspices of the General Secretariat of Science and Technology of Greece.

References

1. Andersson, O. K. Chem Fiber Int 2000, 50, 70.
2. Bagley, E. B. J Appl Phys 1957, 28, 624.
3. Hyun, K. S. Polym Eng Sci 1974, 14, 666.
4. Huang, J. C.; Shen, H. F. Adv Polym Technol 1989, 9, 211.
5. Kamal, M. R.; Nyun, H. Polym Eng Sci 1980, 20, 109.
6. Liang, J.-Z. Polym Test 2000, 19, 289.
7. Penwell, R. C.; Porter, R. S.; Middleman, S. J Polym Sci Part A-2: Pol Physics 1971, 9, 731.
8. Luo, X.-L.; Tanner, R. I. J Non-Newtonian Fluid Mech 1986, 22, 61.
9. Dupont, S.; Crochet, M. J. J Non-Newtonian Fluid Mech 1988, 29, 81.
10. Luo, X.-L.; Mitsoulis, E. J Rheol 1990, 34, 309.
11. Mitsoulis, E.; Hatzikiriakos, S. G. Rheol Acta 2003, 42, 309.
12. Siginer, D. A.; De Kee, D.; Chhabra, R. P. Advances in the Flow and Rheology of Non-Newtonian Fluids; Rheology Series 8; Elsevier: Amsterdam, 1999; Part B, p 1183.
13. Morland, C. D.; Williams, B. Fiber Prod 1980, 32.
14. Kohan, M. I. Nylon Plastics Handbook; Hanser/Gardner: Cincinnati, OH, 1995; Chapter 3.
15. Ciaperoni, A.; Mula, A. Chimica e Tecnologia delle Poliammidi; Pacini Editore: Pisa, Italy, 2001; p 14.
16. ISO Method 307; International Organization for Standardization.
17. Waltz, J. E.; Taylor, G. B. Anal Chem 1947, 19, 448.
18. Kohan, M. I. Nylon Plastics Handbook; Hanser/Gardner: Cincinnati, OH, 1995; Chapter 4.
19. Forsstrom, D.; Reitberger, T.; Terselius, B. Polym Degrad Stab 2000, 67, 255.
20. Kohan, M. I. Nylon Plastics Handbook; Hanser/Gardner: Cincinnati, OH, 1995; Chapter 2.
21. ISO Method 15512; International Organization for Standardization, Geneva, Switzerland, 1994.
22. Macosko, C. W. Rheology Principles, Measurements, and Applications; VCH: Poughkeepsie, NY (1994); Chapter 2.
23. Papanastasiou, A. C.; Scriven, L. E.; Macosko, C. W. J Rheol 1983, 27, 387.
24. Luo, X.-L.; Tanner, R. I. Int J Num Methods Eng 1988, 25,9.
25. Hatzikiriakos, S. G.; Mitsoulis, E. Rheol Acta 1996, 35, 545.
26. Kajiwara, T.; Barakos, G.; Mitsoulis, E. Int J Polym Anal Char 1995, 1, 201.
27. Pezzin, G.; Gechele, G. B. J Appl Polym Sci 1964, 8, 2145.
28. Utracki, L. A.; Catani, A. M.; Bata, G. L.; Kamal, M. R.; Tan, V. J Appl Polym Sci 1982, 27, 1913.
29. Barnes, H. A.; Hutton, J. F.; Walters, K. An Introduction to Rheology; Rheology Series 3; Elsevier: Amsterdam, 1989; Chapter 5.